



**HAL**  
open science

## **Empirical Modelling Using Dummy Atoms (EMUDA): An alternative approach for studying 'auxetic' structures**

Joseph N Grima, Ruben Gatt, Trevor Giles Chircop Bray, Andrew Alderson,  
Kenneth Evans

### ► **To cite this version:**

Joseph N Grima, Ruben Gatt, Trevor Giles Chircop Bray, Andrew Alderson, Kenneth Evans. Empirical Modelling Using Dummy Atoms (EMUDA): An alternative approach for studying 'auxetic' structures. *Molecular Simulation*, 2005, 31 (13), pp.913-922. 10.1080/08927020500401121 . hal-00514968

**HAL Id: hal-00514968**

**<https://hal.science/hal-00514968>**

Submitted on 4 Sep 2010

**HAL** is a multi-disciplinary open access archive for the deposit and dissemination of scientific research documents, whether they are published or not. The documents may come from teaching and research institutions in France or abroad, or from public or private research centers.

L'archive ouverte pluridisciplinaire **HAL**, est destinée au dépôt et à la diffusion de documents scientifiques de niveau recherche, publiés ou non, émanant des établissements d'enseignement et de recherche français ou étrangers, des laboratoires publics ou privés.

## Empirical Modelling Using Dummy Atoms (EMUDA): An alternative approach for studying 'auxetic' structures

Journal:	<i>Molecular Simulation</i> / <i>Journal of Experimental Nanoscience</i>
Manuscript ID:	GMOS-2005-0044.R1
Journal:	Molecular Simulation
Date Submitted by the Author:	05-Oct-2005
Complete List of Authors:	Grima, Joseph; University of Malta, Department of Chemistry Gatt, Ruben; University of Malta, Department of Chemistry Chircop Bray, Trevor; University of Malta, Department of Chemistry alderson, andrew; The University of Bolton, CMRI Evans, Kenneth; University of Exeter, Department of Engineering
Keywords:	Auxetic, honeycomb, modelling, EMUDA, negative Poisson
Note: The following files were submitted by the author for peer review, but cannot be converted to PDF. You must view these files (e.g. movies) online.	
conventional_honeycomb_hinging.gif conventional_honeycomb_stretching.gif reentrant_honeycomb_hinging.gif reentrant_honeycomb_stching.gif	

1  
2  
3 **Empirical Modelling Using Dummy Atoms (EMUDA): An**  
4  
5  
6 **alternative approach for studying ‘auxetic’ structures**  
7  
8  
9

10  
11 JOSEPH N. GRIMA\*<sup>†</sup>, RUBEN GATT<sup>†</sup>, TREVOR G. CHIRCOP BRAY<sup>†</sup>,  
12  
13 ANDREW ALDERSON<sup>‡</sup> and KENNETH E. EVANS<sup>¶</sup>  
14

15  
16  
17 <sup>†</sup> Department of Chemistry, University of Malta, Msida, MSD 05, Malta  
18

19  
20 e-mail: [joseph.grima@um.edu.mt](mailto:joseph.grima@um.edu.mt) - www: <http://home.um.edu.mt/auxetic>  
21

22 <sup>‡</sup> Centre for Materials Research and Innovation, University of Bolton, Bolton, BL3 5AB, UK  
23

24 <sup>¶</sup> Department of Engineering, University of Exeter, Exeter, EX4 4QF, UK.  
25  
26  
27  
28  
29  
30

---

31  
32  
33 **ABSTRACT:**  
34  
35  
36

37  
38 Auxetics (materials or structures) are systems with a negative  
39  
40 Poisson’s ratio, a property that arises from the way various geometric  
41  
42 features in the structure (or internal structure in the case of materials)  
43  
44 deform when subjected to uniaxial loads. Such systems are normally  
45  
46 studied by examining the behaviour of idealised representations of  
47  
48 structures, which deform in a controlled fashion (e.g. deforming solely  
49  
50 through hinging or stretching). Methods used for the analysis typically  
51  
52 involve construction of real physical macro-models and/or derivation  
53  
54 of analytical expressions for the mechanical properties. This paper  
55  
56 proposes an alternative method for analysing such structures whereby  
57  
58  
59  
60

1  
2  
3 idealised ‘hinging’ or ‘stretching’ structures are constructed within a  
4  
5 molecular modelling environment using dummy atoms and examined  
6  
7 using standard molecular mechanics techniques. We will show that this  
8  
9 methodology of ‘empirical modelling using dummy atoms’ (EMUDA)  
10  
11 successfully reproduces the known properties of two-dimensional  
12  
13 conventional and auxetic hexagonal honeycombs hence confirming the  
14  
15 suitability of this technique for studying auxetic structures.  
16  
17  
18  
19  
20  
21  
22

23 *Keywords:* Auxetic; negative Poisson’s ratio; honeycomb; modelling;  
24  
25 EMUDA  
26  
27  
28  
29  
30  
31  
32  
33  
34  
35  
36  
37  
38  
39  
40  
41  
42  
43  
44  
45  
46  
47  
48  
49  
50  
51  
52  
53  
54  
55  
56  
57  
58  
59  
60

## 1. Introduction

The Poisson's ratio is one of the fundamental mechanical properties of materials and describes the changes in shape that result when a material is uniaxially loaded.

Mathematically, the Poisson's ratio of a material in a particular  $Ox_i$ - $Ox_j$  plane for loading in the  $Ox_i$  direction is defined by [1]:

$$\nu_{ij} = -\frac{\text{strain in the orthogonal } Ox_j \text{ direction}}{\text{strain in the axial } Ox_i \text{ direction}} = -\frac{\varepsilon_j}{\varepsilon_i}$$

Equation 1

This property has a positive value in conventional materials since they contract when pulled (i.e. -ve  $\varepsilon_j$  and +ve  $\varepsilon_i$ ) and expand when compressed (i.e. +ve  $\varepsilon_j$  and -ve  $\varepsilon_i$ ). However, the theory of elasticity states that Poisson's ratios can also assume negative values, a property referred to as auxetic behaviour [2] which relates to materials that become wider when stretched and thinner when compressed. In fact, the theory of elasticity suggests that isotropic three-dimensional materials may exhibit Poisson's ratios within the range  $-1 \leq \nu \leq +\frac{1}{2}$  [1]; two-dimensional isotropic systems [3] can exhibit Poisson's ratios within the range  $-1 \leq \nu \leq +1$ ; whilst there are no limits on the Poisson's ratios for anisotropic materials.

Negative Poisson's ratios are known to result in many beneficial enhancements in the properties of materials such as an increased resistance to indentation [4, 5], and improved acoustic absorption properties [6,7]. These benefits make auxetic materials superior to conventional ones for various practical applications, with the result that there is considerable effort aimed at discovering new materials that exhibit auxetic behaviour. In fact, in recent years, auxetic behaviour has

1  
2  
3 been predicted and/or experimentally measured in various types of materials including  
4  
5 foams [8, 12], nano- and micro-structured polymers [2, 13 - 19], cubic metals [20],  
6  
7 silicates [21 - 26] and zeolites [27]. In all of these materials, the negative Poisson's  
8  
9 ratios can be explained in terms of the materials' particular nanostructure (in the case  
10  
11 of the nanostructured polymers, metals, silicates and zeolites) or microstructure (in the  
12  
13 case of the microstructured polymers and foams) and the way these nano/micro-  
14  
15 structures deform when the materials are subjected to uniaxial loads. An important  
16  
17 feature that has emerged from the research in this field is that the Poisson's ratio is a  
18  
19 scale-independent property [4]. In other words, the deformations can take place at the  
20  
21 nano (molecular), micro or even at the macro level as the only requirement for auxetic  
22  
23 behaviour is the right combination of the 'geometry' and the 'deformation  
24  
25 mechanism'. In view of this, a very popular approach for studying auxetic systems is  
26  
27 to study 'idealised structures' which could represent an idealised form of the  
28  
29 nano/micro-structure of a material. These idealised structures can be studied  
30  
31 mathematically by deriving analytical equations for their 'mechanical properties' in  
32  
33 terms of various geometric and structural parameters. Although these analytical  
34  
35 equations are sometimes tedious to derive, once available they provide researchers  
36  
37 with a very important tool for gaining information about the behaviour of these  
38  
39 structures and, more importantly, insight into the behaviour of the real materials  
40  
41 which have nano/micro structures that are similar to these 'idealised structures'.  
42  
43  
44  
45  
46

47  
48 Here we propose an alternative method to deriving analytical equations for  
49  
50 studying 'idealised structures' – a method where the 'structures' are constructed using  
51  
52 'dummy atoms' and then modelled using custom-made force-fields within a  
53  
54 commercially available molecular modelling package. This approach of 'empirical  
55  
56 modelling using dummy atoms' (EMUDA in short) will be tested on systems that  
57  
58  
59  
60

1  
2  
3 have already been extensively studied through analytical modelling (the hexagonal  
4  
5 honeycomb structure [28 - 31]) in an attempt to validate the EMUDA methodology  
6  
7  
8  
9

## 10 11 12 **2. The mechanical properties of hexagonal honeycomb structures**

13  
14  
15  
16 Hexagonal honeycomb structures deforming solely through hinging of the cell walls  
17  
18 (the idealised hinging model) or solely through stretching of the cell walls (the  
19  
20 idealised stretching model) have been extensively studied in view of their potential of  
21  
22 exhibiting auxetic behaviour [28 - 31]. Referring to Fig. 1, it has been shown through  
23  
24 analytical modelling that these systems can exhibit both auxetic and conventional  
25  
26 behaviour, and the sign of the Poisson's ratios depends on both the shape of the  
27  
28 honeycomb and the deformation mechanisms:  
29  
30  
31

32 (a) for  $0^\circ < \theta < 90^\circ$  (i.e. for the re-entrant honeycombs):

$$33 \quad \nu_{12}^{\text{hinging}}, \nu_{21}^{\text{hinging}} = -ve \quad (\text{auxetic behaviour})$$

$$34 \quad \nu_{12}^{\text{stretching}}, \nu_{21}^{\text{stretching}} = +ve \quad (\text{conventional behaviour})$$

35  
36  
37  
38  
39 (b) for  $90^\circ < \theta < 180^\circ$  (i.e. for the non re-entrant honeycombs):

$$40 \quad \nu_{12}^{\text{hinging}}, \nu_{21}^{\text{hinging}} = +ve \quad (\text{conventional behaviour})$$

$$41 \quad \nu_{12}^{\text{stretching}}, \nu_{21}^{\text{stretching}} = -ve \quad (\text{auxetic behaviour})$$

In fact, for the systems illustrated in Fig. 1, the strains in the  $Ox_i$  directions ( $i = 1, 2$ ) for the hinging and stretching modes of deformation are given by:

$$\varepsilon_i^{\text{hinging}} = \frac{1}{X_i} \frac{dX_i}{d\theta} d\theta \quad \& \quad \varepsilon_i^{\text{stretching}} = \frac{1}{X_i} \frac{dX_i}{dl} dl, \quad i = 1, 2$$

**Equations 2**

where  $X_1$  and  $X_2$  are dimensions of the unit cell along the  $Ox_1$  and  $Ox_2$  directions which are given by:

$$X_1 = 2l \sin(\theta) \quad \& \quad X_2 = 2(h - l \cos(\theta))$$

**Equations 3**

and the analytical equations for the on-axis Poisson's ratios (from Equation 1 to Equations 3) and Young's moduli for these hexagonal honeycomb systems are given by [30, 31]:

For the Hinging model:

$$\nu_{12}^{\text{hinging}} = \frac{1}{\nu_{21}^{\text{hinging}}} = -\frac{\varepsilon_2^{\text{hinging}}}{\varepsilon_1^{\text{hinging}}} = -\tan(\theta) \frac{X_1}{X_2}$$

**Equations 4**

$$E_1^{\text{hinging}} = \frac{K_h}{bl^2 \cos^2(\theta)} \frac{X_1}{X_2} \quad \& \quad E_2^{\text{hinging}} = \frac{K_h}{bl^2 \sin^2(\theta)} \frac{X_2}{X_1}$$

**Equations 5**

For the Stretching model:

$$\nu_{12}^{\text{stretching}} = -\frac{\varepsilon_2^{\text{stretching}}}{\varepsilon_1^{\text{stretching}}} = \cot(\theta) \frac{X_1}{X_2} \quad \& \quad \nu_{21}^{\text{stretching}} = -\frac{\varepsilon_1^{\text{stretching}}}{\varepsilon_2^{\text{stretching}}} = \frac{\sin \theta \cos \theta}{2 + \cos^2 \theta} \frac{X_2}{X_1}$$

**Equations 6**

$$E_1^{\text{stretching}} = \frac{K_s}{b \sin^2(\theta)} \frac{X_1}{X_2} \quad \& \quad E_2^{\text{stretching}} = \frac{K_s}{b(2 + \cos^2(\theta))} \frac{X_2}{X_1}$$

Equations 7

where:

$\frac{X_1}{X_2}$  is the ratio of the unit cell dimensions  $X_1$  and  $X_2$  which is given by:

$$\frac{X_1}{X_2} = \frac{2l \sin(\theta)}{2(h - l \cos(\theta))} = \frac{\sin(\theta)}{h/l - \cos(\theta)}$$

Equation 8

$b$  is the thickness of the honeycombs in the third dimension;

$K_h$  is the hinging force constant governing the resistance to ‘hinging’ of the ‘ $\theta$  hinges’ defined in the usual way, i.e.  $M = K_h \delta\theta$ , where  $M$  is the magnitude of the moment applied to the arm and  $\delta\theta$  is the angular displacement of the arm of the honeycomb;

$K_s$  is the stretching force constant governing the resistance to ‘stretching’ of the elements of the honeycombs defined in the usual way, i.e.  $F = K_s \delta s$ , where  $F$  is the magnitude of the force applied along the length of a honeycomb element of length  $s$  and  $\delta s$  is the change in length of the element.

--- Insert Fig. 1 here ---

1  
2  
3 The equations confirm that the Poisson's ratios are independent of scale and depend  
4 only on the ratio the lengths of the honeycomb cell walls,  $h/l$ , the angle  $\theta$  between  
5 the cell walls (i.e. the geometry of the honeycomb) and the type of deformation  
6 mechanism (i.e. whether the system deforms through 'idealised hinging' or 'idealised  
7 stretching'). The equations also suggest that the magnitudes of the Young's moduli  
8 depend on scale, i.e. on the magnitude of  $b$  and  $l$ , but there are no restrictions on the  
9 range of values these geometric parameters can take.  
10  
11  
12  
13  
14  
15  
16  
17  
18  
19  
20  
21  
22  
23  
24

### 25 **3. The EMUDA methodology**

26  
27  
28  
29

30 The lack of restrictions on the scale at which the idealised honeycombs can be  
31 constructed permits the construction of these 'honeycomb structures' at any scale  
32 including the nanometre scale, where they can be modelled using force-field based  
33 molecular modelling packages such as *Cerius*<sup>2</sup>. In such an environment, these  
34 idealised systems can be constructed by inserting 'dummy atoms' at the vertices of the  
35 honeycombs and connecting these by 'bonds' that would represent the 'ribs' of the  
36 honeycombs. In this particular case, an infinite sheet of a honeycomb system may be  
37 constructed within *Cerius*<sup>2</sup> through the use of periodic boundary conditions where one  
38 unit cell contains four dummy atoms as illustrated in Fig. 2.  
39  
40  
41  
42  
43  
44  
45  
46  
47  
48  
49  
50  
51  
52  
53  
54  
55  
56  
57  
58  
59  
60

--- Insert Fig. 2 here ---

The shape and size of the honeycomb may be controlled by adjusting the magnitude of the distances and angles between connected atoms. This can be done by first labelling the dummy atoms in such a way that the different lengths/angles in the system may be uniquely identified (in this particular case, referring to Fig. 2, the dummy atoms may be labelled using two different labels, A and B<sup>1</sup>) and then listing the variables that need to be monitored during the simulation. Referring to Fig. 1 and Fig. 2, in this particular case, these variables are:

- (i) the bond lengths  $|AA|$ ,  $|BB|$  and  $|AB|$ , which for an unloaded honeycomb, their values should be equal to
 
$$|AA|_0 = |BB|_0 = h \text{ and } |AB|_0 = l ;$$
- (ii) the bond angles  $|A\hat{A}B|$  and  $|A\hat{B}B|$ , which for an unloaded honeycomb, their values should be equal to
 
$$|A\hat{A}B|_0 = |A\hat{B}B|_0 = \theta ;$$
- (iii) the torsion angles  $\phi$  between four connected atoms X-X-X-X, where X can be A or B, which must be set to  $0^\circ$  or  $\pm 180^\circ$  (a requirement for constraining the honeycomb system to stay planar).

The ‘rules’ for describing the behaviour of these variables can now be coded in a custom-made force-field file that involves bond-terms but no VDW or Coulombic

<sup>1</sup> It should be noted that the simplified labelling system using only two different ‘atom types’ (A and B) as illustrated in Fig. 2b could be used since this simplified labelling system still permits the differentiation between the ‘bonds’ of length  $l$  (i.e. bonds A-B) from the ‘bonds’ of length  $h$  (i.e. bonds A-A and B-B) whilst all the A-B-B and A-A-B bond angles refer to  $\theta$ -angles.

interactions (or through the use of ‘restraints’). Such a force-field file must contain all the necessary information for setting up the ‘energy expression’ of this ‘molecule’ (or rather a ‘mechanical system’ that obeys the classical laws of physics). In this particular case, an equation for the ‘potential energy’ of the system can be written in the form [32]:

$$\begin{aligned}
 E = & \sum_{\substack{\text{all AB} \\ \text{bonds}}} \frac{1}{2} k_s (|AB| - |AB|_0)^2 + \sum_{\substack{\text{all AA} \\ \text{bonds}}} \frac{1}{2} k_s (|AA| - |AA|_0)^2 + \sum_{\substack{\text{all BB} \\ \text{bonds}}} \frac{1}{2} k_s (|BB| - |BB|_0)^2 \\
 & + \sum_{\substack{\text{all ABB} \\ \text{bond angles}}} \frac{1}{2} k_h (|\hat{A}\hat{B}\hat{B}| - |\hat{A}\hat{B}\hat{B}|_0)^2 + \sum_{\substack{\text{all AAB} \\ \text{bond angles}}} \frac{1}{2} k_h (|\hat{A}\hat{A}\hat{B}| - |\hat{A}\hat{A}\hat{B}|_0)^2 \\
 & + \sum_{\substack{\text{all X-X-X-X} \\ \text{torsion angles}}} \frac{1}{2} k_t [1 - \cos(2\phi)]
 \end{aligned}$$

Equation 9

where the ‘spring constants’  $k_s$ ,  $k_h$  and  $k_t$  define the resistance to ‘stretching’ (i.e. changes in bond lengths), ‘hinging’ (i.e. changes in bond angles), and ‘going out of plane’ respectively. Since the honeycomb systems are required to remain planar,  $k_t$  must be set as high as possible. Furthermore, it is possible to make the ‘stretching’ or ‘hinging’ mechanism predominate by setting  $k_h \gg k_s$  (for systems deforming primarily through stretching of the ‘ribs’ (i.e. stretching of the ‘bonds’)), or by setting  $k_s \gg k_h$  (for systems deforming primarily through hinging of the ‘ $\theta$ -hinges’).

Having set up the energy expression, the structures can be optimised (‘minimised’) using one of the minimisation algorithms in the modelling package so as to obtain the conformation with the lowest energy where the various bond lengths and angles will become equal, or as close as possible, to their respective ideal values that are defined in the force-field. The mechanical properties of the system can then be simulated using standard techniques for simulating the mechanical properties of

1  
2  
3 molecular systems [32]. In *Cerius*<sup>2</sup>, this can be done in a number of ways, including  
4  
5 by computing the stiffness matrix **C** and its inverse, the compliance matrix **S** from the  
6  
7 second derivative of the energy expression since:  
8

$$c_{ij} = \frac{1}{V} \frac{\partial^2 E}{\partial \varepsilon_i \partial \varepsilon_j} \quad i, j = 1, 2, \dots, 6,$$

9  
10  
11  
12  
13  
14  
15 **Equation 10**

16 where *V* is the volume of the unit cell and  $\varepsilon_i$  are strain components. Other mechanical  
17  
18 properties (including the on- and off-axis Poisson's ratios) can then be calculated  
19  
20 from these matrices. Furthermore these periodic systems can be minimised with  
21  
22 externally applied uniaxial stresses, a procedure that is particularly useful for the  
23  
24 visualisation of the deformations in the structure that result from an externally applied  
25  
26 uniaxial load.  
27  
28  
29  
30  
31  
32  
33

#### 34 **4. Testing of the EMUDA methodology through modelling of various 'idealised** 35 36 **hinging' or 'idealised stretching' honeycombs**

##### 37 38 39 **4.1 Methods used:**

40  
41  
42 The simulations were performed using *Cerius*<sup>2</sup> V3.0 (Molecular Simulations Inc., San  
43  
44 Diego USA) on an O2 R5000 SGI workstation and involved: (a) the construction of  
45  
46 the unminimised honeycomb structure within the molecular modelling environment;  
47  
48 (b) writing of the custom-made force-field files; and (c) the calculations, i.e., the  
49  
50 simulation of the minimum energy structure and the calculation of the mechanical  
51  
52 properties.  
53  
54  
55  
56  
57  
58  
59  
60

1  
2  
3 (a) *Construction of the unminimised model*: An ‘unminimised’ honeycomb model was  
4  
5 constructed through the graphical interface and the ‘Crystal Builder’ module of  
6  
7 *Cerius<sup>2</sup>* using four dummy atoms per unit cell, which were assigned force-field types  
8  
9 ‘A’ and ‘B’ as illustrated in Fig. 2. The honeycomb was aligned along the YZ-plane  
10  
11 (that contains the (100) plane of the unit cell) with ‘bonds’ of length  $h$  aligned parallel  
12  
13 to the Z-axis (that corresponds to the [001] direction). This construction results in an  
14  
15 infinite number of tessellates of ‘honeycombs’ down the X-direction, which were kept  
16  
17 aligned with each other at a separation of 1 Å during the simulation. This was done by  
18  
19 constraining the unit cell parameters  $a$ ,  $\beta$  and  $\gamma$  to remain ‘fixed’ during the simulation  
20  
21 at 1 Å, 90° and 90° respectively whilst allowing  $b$ ,  $c$  and  $\alpha$  to vary.  
22  
23  
24  
25  
26  
27

28 (b) *Construction of the custom-made force-field files*: Twelve different force-field  
29  
30 files were constructed with different combinations of  $(h, l)$ ,  $(k_h, k_s)$  and  $\theta$  as listed in  
31  
32 Table 1. These force-field files describe honeycomb structures that deform solely, (in  
33  
34 practice predominantly), through hinging of the  $\theta$ -angles or through stretching of the  
35  
36 ‘bonds’ (the honeycomb ribs), where, referring to Table 1, the force-field files with  
37  
38  $(k_h, k_s) = (50 \text{ kcal mol}^{-1} \text{ rad}^{-2}, 10,000 \text{ kcal mol}^{-1} \text{ Å}^{-1})$  were designed to describe the  
39  
40 ‘idealised hinging structures’, since  $k_h \ll k_s$ , whilst the force-field files with  $(k_h, k_s) =$   
41  
42  $(10,000 \text{ kcal mol}^{-1} \text{ rad}^{-2}, 50 \text{ kcal mol}^{-1} \text{ Å}^{-2})$  were designed to describe the ‘idealised  
43  
44 stretching structures’, since  $k_h \gg k_s$ . In all simulations,  $k_t$  was set at the maximum  
45  
46 value permitted by the software (999 kcal mol<sup>-1</sup>).  
47  
48  
49

50 Note that to avoid cumbersome conversion factors, the ‘stiffness constants’  
51  
52 will be given in kcal mol<sup>-1</sup> rad<sup>-2</sup> (for angles) or kcal mol<sup>-1</sup> Å<sup>-2</sup> (for lengths), while  
53  
54 lengths will be given in Å. The units of the stiffness constants relate to one mole ( $N_A =$   
55  
56  
57  
58  
59  
60

6.022 × 10<sup>23</sup>) of angles or lengths, and can be converted to SI units through the conversion factors listed in Appendix I.

--- Insert Table 1 here ---

(c) *Calculations*: For each of these twelve force-field files, the unminimised structure was first minimised using the SMART minimiser up to the default *Cerius*<sup>2</sup> high convergence criteria, which includes a condition that the RMS force must be less than 0.001 kcal mol<sup>-1</sup> Å<sup>-1</sup>. The numerical values of the mechanical properties were calculated using the second derivative method. This produced the full 6×6 stiffness and compliance matrices. However, since the honeycombs are two-dimensional systems aligned in the YZ-plane, only a sub-section of the full 6×6 stiffness and compliance matrices are of interest, namely the 3×3 sub-matrix, which relate solely to Y and Z directions. These 3×3 stiffness and compliance ‘sub-matrices’ relate stress to strain for a 2D system in the YZ-plane and are defined through:

$$\begin{pmatrix} \sigma_y \\ \sigma_z \\ \tau_{yz} \end{pmatrix} = \begin{pmatrix} c_{22} & c_{23} & c_{24} \\ c_{32} & c_{33} & c_{34} \\ c_{42} & c_{43} & c_{44} \end{pmatrix} \begin{pmatrix} \varepsilon_y \\ \varepsilon_z \\ \gamma_{yz} \end{pmatrix} \quad \& \quad \begin{pmatrix} \varepsilon_y \\ \varepsilon_z \\ \gamma_{yz} \end{pmatrix} = \begin{pmatrix} s_{22} & s_{23} & s_{24} \\ s_{32} & s_{33} & s_{34} \\ s_{42} & s_{43} & s_{44} \end{pmatrix} \begin{pmatrix} \sigma_y \\ \sigma_z \\ \tau_{yz} \end{pmatrix},$$

**Equations 11**

where the terms  $c_{ij}$  and  $s_{ij}$  in the 3×3 matrices refer to the respective terms in the original 6×6 matrices.

The Young’s moduli  $E_y$  and  $E_z$  for loading in Y- and Z-directions respectively and the in-plane on-axis Poisson’s ratios  $\nu_{yz}$  and  $\nu_{zy}$  for loading in Y- and Z-directions can be calculated from the terms in the compliance matrix, and are given by:

$$E_y = \frac{\sigma_y}{\varepsilon_y} = \frac{1}{s_{22}} \quad E_z = \frac{\sigma_z}{\varepsilon_z} = \frac{1}{s_{33}}$$

$$V_{yz} = -\frac{\varepsilon_z}{\varepsilon_y} = -\frac{s_{32}}{s_{22}} \quad V_{zy} = -\frac{\varepsilon_y}{\varepsilon_z} = -\frac{s_{23}}{s_{33}}$$

Equations 12

In addition to these second derivative calculations, minimisations of these systems at various uniaxially applied external loads were also performed in an attempt to ‘visualise’ the effect of stress on the various geometric parameters of these systems.

Finally, it should be noted that the unit cell used in these simulations, i.e. the one which contains only four atoms, is the smallest rectangular unit cell for such systems. In order to ensure that the quality of the results obtained were independent of the unit cell, a convergence test was carried out where a selection of the simulations were repeated with ‘superlattices’ of (2x2) and (4x4) units containing 16 and 64 dummy atoms per unit cell respectively.

#### **4.2 Results and discussion:**

All the ‘energy minimisations’ and ‘second derivative calculations’ with the smallest unit cells were observed to proceed to completion in less than two minutes on the SGI O2 workstation. However, the simulation time was considerably longer when the larger unit cells were used as illustrated in Table 2. This increase in the computational time did not result in any significant differences in the values of the on-axis mechanical properties (see **Table 2**, and hence it may be concluded that the smallest

1  
2  
3 unit cell containing only four ‘dummy atoms’ is a suitable representation for this  
4  
5 infinite system for simulations of this type.  
6  
7  
8  
9

10 --- Insert Table 2 here ---  
11

12 Images illustrating the deformations for a selection of the honeycombs as a  
13 result of the uniaxially applied loads are shown in Fig. 3 and in the supplementary  
14 information in electronic format (where they are shown as an animation). These  
15 images illustrate very clearly that the ‘hinging re-entrant’ and the ‘stretching non re-  
16 entrant’ honeycombs exhibit auxetic behaviour, whilst the ‘hinging non re-entrant’  
17 and the ‘stretching re-entrant’ honeycombs exhibit conventional behaviour.  
18  
19  
20  
21  
22  
23  
24

25 These observations are confirmed by the numerical values of the Poisson’s  
26 ratios obtained from the second derivative method (*see* Table 3). A comparison of the  
27 simulated on-axis Poisson’s ratios and Young’s moduli with the equivalent values as  
28 predicted by the analytical models described in section 2 suggests that the values of  
29 the Poisson’s ratios and moduli simulated through the EMUDA method are generally  
30 in very close agreement with those predicted by the analytical models (within  $\pm 3\%$  in  
31 the case of the stretching models and within  $\pm 11\%$  in the case of the hinging models,  
32 *see* Table 3). In this respect, it should be noted that the extent of agreement of the  
33 EMUDA simulated mechanical properties to those predicted by the analytical models  
34 is related to the magnitude of the Young’s moduli (*see* Fig. 4), and in fact, the  
35 properties of the ‘stretching models’ compared better with the analytical model than  
36 the ‘hinging models’ as a result of the lower moduli of the ‘stretching models’. This  
37 relationship between the ‘quality of the EMUDA results’ and the moduli can be  
38 explained by the fact that an increase in the Young’s modulus as predicted by the  
39 analytical expression of the idealised structures signifies that the structures are not  
40  
41  
42  
43  
44  
45  
46  
47  
48  
49  
50  
51  
52  
53  
54  
55  
56  
57  
58  
59  
60

easily deformed through the desired mode of deformation. In such scenarios, the assumption that the ‘desired mode of deformation’ is the ‘predominant mode of deformation’ can no longer be made as other modes of deformation start to compete effectively with the desired one.

--- Insert Fig. 3 here ---

--- Insert Table 3 here ---

--- Insert Fig. 4 here ---

In fact, one could argue that the scenarios studied here, i.e. where the honeycomb structures deform solely through ‘hinging’ or through ‘stretching’ represent unrealistic and highly idealised scenarios, as in reality, one would expect that there is superposition of effects given by stretching and hinging of the ribs<sup>2</sup>. In such systems, for loading by a stress  $\sigma_i$  in an  $Ox_i$  ( $i = 1,2$ ) direction, the strains in the  $Ox_i$  direction are given by:

$$\varepsilon_i^{\text{stretching + hinging}} = \varepsilon_i^{\text{stretching}} + \varepsilon_i^{\text{hinging}}$$

**Equation 13**

where  $\varepsilon_i^{\text{stretching}}$  is the strain due to stretching and  $\varepsilon_i^{\text{hinging}}$  is the strain due to hinging.

But since a strain  $\varepsilon_i$  in an  $Ox_i$  direction is related to a stress  $\sigma_i$  in the same direction through:

$$\varepsilon_i = \frac{1}{E_i} \sigma_i$$

**Equation 14**

<sup>2</sup> In reality, one would also expect that the ‘rod elements’ will ‘flex’ to some extent, but the flexure mode of deformation [29] is not being included in these simulations due to the difficulty to represent flexure through the EMUDA methodology.

where  $E_i$  is the Young's modulus in the  $Ox_i$  direction, then from Equation 13 and Equation 14:

$$\frac{\sigma_i}{E_i^{\text{stretching + hinging}}} = \frac{\sigma_i}{E_i^{\text{stretching}}} + \frac{\sigma_i}{E_i^{\text{hinging}}}$$

Equation 15

where  $E_i^{\text{stretching + hinging}}$  is the Young's modulus in the  $Ox_i$  direction due to concurrent stretching and hinging,  $E_i^{\text{stretching}}$  is the Young's modulus in the  $Ox_i$  direction due to stretching given by Equations 7 whilst  $E_i^{\text{hinging}}$  is the Young's modulus in the  $Ox_i$  direction due to hinging given by Equations 5.

By rearranging Equation 15, the Young's modulus for loading in an  $Ox_i$  direction ( $i = 1, 2$ ) for systems deforming through concurrent stretching and hinging is given by:

$$E_i^{\text{stretching + hinging}} = \frac{E_i^{\text{stretching}} \cdot E_i^{\text{hinging}}}{E_i^{\text{stretching}} + E_i^{\text{hinging}}}$$

Equation 16

Furthermore, since from Equation 1 the strain in the orthogonal  $Ox_j$  direction are given by:

$$\varepsilon_j = -\nu_{ji}\varepsilon_i = \frac{-\nu_{ji}}{E_i}\sigma_i$$

Equation 17

and since in analogy to Equation 13:

$$\varepsilon_j^{\text{stretching + hinging}} = \varepsilon_j^{\text{stretching}} + \varepsilon_j^{\text{hinging}}$$

Equation 18

then from Equation 17 and Equation 18:

$$\frac{-\nu_{ij}^{\text{stretching + hinging}} \cdot \sigma_i}{E_i^{\text{stretching + hinging}}} = \frac{-\nu_{ij}^{\text{stretching}} \cdot \sigma_i}{E_i^{\text{stretching}}} + \frac{-\nu_{ij}^{\text{hinging}} \cdot \sigma_i}{E_i^{\text{hinging}}}$$

Equation 19

where  $\nu_{ij}^{\text{stretching + hinging}}$  is the Poisson's ratio in the  $Ox_i-Ox_j$  plane for loading in the  $Ox_i$  direction due to concurrent stretching and hinging,  $\nu_{ij}^{\text{stretching}}$  is the Poisson's ratio in the  $Ox_j-Ox_j$  plane for loading in the  $Ox_i$  direction due to stretching given by Equations 6 whilst  $\nu_{ij}^{\text{hinging}}$  is the Poisson's ratio in the  $Ox_i-Ox_j$  plane for loading in the  $Ox_i$  direction due to hinging given by Equations 4.

By rearranging Equation 19, the Poisson's ratio in the  $Ox_i-Ox_j$  plane for loading in the  $Ox_i$  direction ( $i, j = 1, 2$ ) for systems deforming through concurrent stretching and hinging is given by:

$$\nu_{ij}^{\text{stretching + hinging}} = \frac{\nu_{ij}^{\text{stretching}} E_i^{\text{hinging}} + \nu_{ij}^{\text{hinging}} E_i^{\text{stretching}}}{E_i^{\text{stretching}} + E_i^{\text{hinging}}}$$

Equation 20

In an attempt to assess the suitability of the EMUDA modelling technique for simulating such more realistic systems, the simulations described in section 4.1 were repeated with force constants  $(k_h, k_s) = (50 \text{ kcal mol}^{-1} \text{ rad}^{-2}, 50 \text{ kcal mol}^{-1} \text{ \AA}^{-2})$ . As illustrated in Table 4, the simulated values of the moduli and Poisson's ratios for these

1  
2  
3 'concurrent stretching and hinging' systems compare extremely well with those  
4  
5 predicted by the analytical model derived here and given by Equation 16 and Equation  
6  
7 20 (within  $\pm 1\%$ , generally the EMUDA Poisson's ratios agree to the values of the  
8  
9 analytical model to the 4<sup>th</sup> decimal place).  
10  
11

12  
13  
14 All this is very significant as it confirms that the EMUDA technique is suitable for  
15  
16 simulating the mechanical properties of these structures, and in particular, it can be  
17  
18 used easily and successfully to:  
19

- 20 (1) assess whether a particular idealised structure constructed from  
21  
22 'rods' deforming **solely** through 'hinging' or 'stretching' exhibits  
23  
24 conventional or auxetic behaviour, and to what extent it does so;  
25  
26
- 27 (2) determine how changes in the geometric and structural  
28  
29 characteristics affect the mechanical properties;  
30  
31
- 32 (3) visualise and measure the effect of stresses on the geometry of  
33  
34 these structures and hence elucidate the 'deformation  
35  
36 mechanism/s';  
37  
38
- 39 (4) **simulate more realistic systems constructed from 'rods' which**  
40  
41 **deform through 'concurrent hinging and stretching' (i.e. it can**  
42  
43 **simulate the superposition of effects given by stretching and**  
44  
45 **hinging of the rods).**  
46

47  
48 In other words, the EMUDA technique offers an excellent alternative to the  
49  
50 construction of analytical expressions and/or real physical models that can be tedious,  
51  
52 expensive and/or time consuming to derive or produce (**especially by chemists who**  
53  
54 **may be more familiar with molecular modelling techniques than with techniques**  
55  
56 **relating to modelling of 'structures'**). In this respect, it should be noted that EMUDA  
57  
58  
59  
60

1  
2  
3 models offer the advantage that they combine the strengths of physical models and  
4 analytical expression in the sense that like the analytical models (but unlike the real  
5 physical models), the EMUDA models can be very easily modified to study the effect  
6 of changes in the various structural characteristics (a new physical model would need  
7 to be constructed for each modification introduced), and like the physical models (but  
8 unlike the analytical models) the EMUDA models allows the user to immediately and  
9 easily ‘visualise’ the changes in the shape and size of the structure.  
10  
11  
12  
13  
14  
15  
16  
17

18  
19 However, the real strength of this new technique is that it is not restricted to  
20 the study honeycomb of systems and it may be used to simulate the properties of  
21 virtually any system composed from rods that deforms through hinging or stretching.  
22 This is very significant as it provides researchers with a quick, easy and inexpensive  
23 alternative for studying structures that could potentially exhibit negative Poisson’s  
24 ratios. In this respect, it is important to note that the observation that the quality of  
25 simulated results improves as the Young’s moduli are lowered suggests that when  
26 modelling novel systems, care should be taken that the parameters are chosen in such  
27 a way that the moduli are kept low. (For example, these simulations suggest that if the  
28 moduli of planar parallel systems arranged at  $1\text{Å}$  to each other in the  $YZ$ -plane are  
29 lower than  $10^4$  GPa, then the simulated properties will be accurate within  $\pm 10\%$ , *see*  
30 Table 4. Note that these values of the moduli refer to planar parallel systems arranged  
31 at  $1\text{Å}$  to each other in the third direction.)  
32  
33  
34  
35  
36  
37  
38  
39  
40  
41  
42  
43  
44  
45  
46  
47

48 It should also be noted that this work suggests that molecular modelling  
49 programs could be easily transformed into tools that may be used by architects and  
50 structural engineers for visualising and analysing structures/mechanisms and to  
51 understand how the structures behave when subjected to mechanical loads, **in the**  
52 **same way that finite element (FE) modelling software normally used by engineers has**  
53  
54  
55  
56  
57  
58  
59  
60

1  
2  
3 been successfully used to model molecular systems (e.g. carbon single-walled  
4  
5 nanotubes [33, 34]). We hope that this will encourage software manufacturers to put  
6  
7 more effort into the design of ‘molecular modelling packages’ in view of the  
8  
9 increased marketability of ‘modified versions’ of these packages.  
10  
11

## 12 13 14 **5. Conclusions**

15  
16  
17  
18 This work has shown that the effect of mechanical loads on the shape of structures  
19  
20 composed from rods that deform through relative changes of the angles between the  
21  
22 rods (i.e. hinging of the rods) or stretching of the rods can be modelled using standard  
23  
24 force-field based molecular modelling methods through a technique, which is being  
25  
26 referred to as ‘Empirical Modelling Using Dummy Atoms’ (EMUDA). It has also  
27  
28 been shown that this EMUDA technique can reproduce the properties of conventional  
29  
30 and auxetic hexagonal honeycombs deforming through stretching or hinging of the  
31  
32 ribs of the honeycomb to an acceptable level of accuracy, which is dependent on the  
33  
34 stiffness of the honeycombs. All this suggests that the EMUDA technique is likely to  
35  
36 offer a very effective alternative for studying the properties of novel ‘auxetic’ systems  
37  
38 that very frequently are assumed to deform in such ways (i.e. through hinging or  
39  
40 stretching) without the need of constructing more expensive real physical models or to  
41  
42 derive analytical expressions for the Poisson’s ratios, with the result that it will  
43  
44 facilitate the discovery, analysis and development of new auxetic systems.  
45  
46  
47  
48  
49

## 50 51 52 **Acknowledgements**

53  
54 The work of Pierre-Sandre Farrugia is gratefully acknowledged.  
55  
56  
57  
58  
59  
60

## Appendix I

The units as used in the EMUDA simulations can be converted to SI to be compared with the analytical equations in section 2 through the conversion factors given in Table 5.

--- Insert table 5 here ---

## Reference:

- 1 B.M. Lempriere. Poisson's ratio in orthotropic materials. *AIAA J.*, **6**, 2226 (1968).
- 2 K.E. Evans, M.A. Nkansah, I.J. Hutchinson, S.C. Rogers. Molecular network design. *Nature*, **353**, 124 (1991).
- 3 K. W. Wojciechowski. Remarks on "Poisson ratio beyond the limits of the elasticity theory". *J. Phys. Soc. Jpn.*, **72**, 1819 (2003).
- 4 A. Alderson. A triumph of lateral thought. *Chem. Ind.*, **10**, 384 (1999).
- 5 R.S. Lakes, K. Elms. Indentability of conventional and negative Poisson's ratio foams. *J. Compos. Mater.*, **27**, 1193 (1993).
- 6 F. Scarpa, W.A. Bullough, P. Lumley. Trends in acoustic properties of iron particle seeded auxetic polyurethane foam. *P.I. Mech. Eng C - J. Mech. Engin. Sci.*, **218**, 241 (2004).
- 7 F. Scarpa, F.C. Smith. Passive and MR fluid-coated auxetic PU foam - Mechanical, acoustic, and electromagnetic properties. *J. Intel. Mat. Syst. Str.*, **15**, 973 (2004).
- 8 R. Lakes. Foam structures with a negative Poisson's ratio. *Science*, **235**, 1038 (1987).
- 9 K.E. Evans, M.A. Nkansah, I.J. Hutchinson. Auxetic foams - modeling negative Poisson's ratios. *Acta Metall. Mater.*, **42**, 1289 (1994).
- 10 N. Gaspar, C.W. Smith, E. A. Miller, G. T. Seidler, K. E. Evans. Quantitative analysis of the microscale of auxetic foams. *Phys. stat. Sol (b)*, **242**, 550 (2005).
- 11 C.W. Smith, J.N. Grima, K.E. Evans. A novel mechanism for generating auxetic behaviour in reticulated foams: Missing rib foam model. *Acta Materiala*, **48**, 4349 (2000).

- 1  
2  
3 12 J.N. Grima, A. Alderson, K.E. Evans. An alternative explanation for the negative  
4 Poisson's ratios in auxetic foams, *J. Phys. Soc. Jpn.*, **74**, 1341 (2005).  
5  
6  
7 13 A.P. Pickles, K.L. Alderson, K.E. Evans. The effects of powder morphology on  
8 the processing of auxetic polypropylene (PP of negative Poisson's ratio). *Polym.*  
9  
10  
11  
12 *Eng. & Sci.*, **36**, 636 (1996).  
13  
14 14 K.L. Alderson, K.E. Evans. Strain-dependent behavior of microporous  
15 polyethylene with a negative Poisson ratio. *J. Mater. Sci.* **28**, 4092 (1993).  
16  
17 15 K.E. Evans, B.D. Caddock. Microporous materials with negative poisson ratios .2.  
18 Mechanisms and interpretation. *J. Phys. D: Appl. Phys.*, **22**, 1877 (1989).  
19  
20  
21 16 J.N. Grima, J.J. Williams, K.E. Evans. Networked calix[4]arene polymers with  
22 unusual mechanical properties. *Chem. Comm.*, DOI 0.1039/b505839b (2005).  
23  
24  
25 17 J.N. Grima, K.E. Evans. Self expanding molecular networks. *Chem. Comm.*, **16**,  
26  
27  
28  
29  
30  
31  
32 18 R.H. Baughman, D.S. Galvao. Crystalline networks with unusual predicted  
33 mechanical and thermal-properties. *Nature*, **365**, 735 (1993).  
34  
35  
36 19 C.B. He, P.W. Liu, A.C. Griffin. Toward negative Poisson ratio polymers through  
37 molecular design, *Macromolecules*, **31**, 3145 (1998).  
38  
39  
40  
41 20 R.H. Baughman, J.M. Shacklette, A.A. Zakhidov, S. Stafstrom. Negative  
42 Poisson's ratios as a common feature of cubic metals. *Nature*, **392**, 362 (1998).  
43  
44  
45 21 A. Yeganeh-Haeri, D.J. Weidner, J. B. Parise. Elasticity of alpha-cristobalite - a  
46 silicon dioxide with a negative Poisson's ratio. *Science*, **257**, 650 (1992).  
47  
48  
49 22 N. R. Keskar, J.R. Chelikowsky. Negative Poisson ratios in crystalline SiO<sub>2</sub> from  
50 1st-principles calculations. *Nature*, **358**, 222 (1992).  
51  
52  
53  
54 23 A. Alderson, K.L. Alderson, K.E. Evans, J.N. Grima, M. Williams. Modelling of  
55 Negative Poisson's Ratio Nanomaterials: Deformation Mechanisms, Structure-  
56  
57  
58  
59  
60

- 1  
2  
3 Property Relationships and Applications. *J. Metastable Nanocryst. Mater.*, **23**, 55,  
4  
5 (2005).  
6  
7  
8 24 A. Alderson, K.E. Evans. Rotation and dilation deformation mechanisms for  
9  
10 auxetic behaviour in the alpha-cristobalite tetrahedral framework structure. *Phys.*  
11  
12 *Chem. Miner.*, **28**, 711 (2001).  
13  
14 25 A. Alderson, K.L. Alderson, K.E. Evans, J.N. Grima, M.R. Willams, P.J. Davies.  
15  
16 Modelling the deformation mechanisms, structure-property relationships and  
17  
18 applications of auxetic nanomaterials. *Phys. Status Solidi B*, **242**, 499 (2005).  
19  
20  
21 26 J.N. Grima, R. Gatt, A. Alderson, K.E. Evans. On the origin of auxetic behaviour  
22  
23 in the silicate  $\alpha$ -cristobalite. *J. Mater. Chem.*, DOI: 10.1039/b508098c (2005).  
24  
25  
26 27 J.N. Grima, R. Jackson, A. Alderson, K.E. Evans. "Do zeolites have negative  
27  
28 Poisson's ratios?" *Advanced Materials*, **12**, 1912 (2000).  
29  
30  
31 28 F.K. Abd el-Sayed, R. Jones, I.W. Burgens. Theoretical approach to the  
32  
33 deformation of honeycomb based composite-materials. *Composites*, **10**, 209  
34  
35 (1979).  
36  
37  
38 29 L.J. Gibson, M.F. Ashby. Cellular Solids: Structure and Properties, Oxford:  
39  
40 Pergamon, Oxford (1988).  
41  
42  
43 30 I.G. Masters, K.E. Evans. Models for the elastic deformation of honeycombs.  
44  
45 *Compos. Struct.*, **35**, 403 (1996).  
46  
47  
48 31 K.E. Evans, A. Alderson, F.R. Christian. Auxetic 2-dimensional polymer  
49  
50 networks - an example of tailoring geometry for specific mechanical - properties.  
51  
52 *J. Chem. Soc. Faraday T.*, **91**, 2671 (1995).  
53  
54  
55 32 Cerius<sup>2</sup>, 'Force-field Based Simulations' and 'Property prediction' User Guides,  
56  
57  
58 Molecular Simulations Inc., San Diego (1997).  
59  
60

- 1  
2  
3 33 C. Li and T.W. Chou. Elastic properties of single-walled carbon nanotubes in  
4  
5 transverse directions, *Phys. Rev. B*, **69**, 073401 (2004).  
6  
7  
8 34 K.I. Tserpesa, P. Papanikos. Finite element modeling of single-walled carbon  
9  
10 nanotubes. *Composites: Part B*, **36**, 468 (2005).  
11  
12  
13  
14  
15  
16  
17  
18  
19  
20  
21  
22  
23  
24  
25  
26  
27  
28  
29  
30  
31  
32  
33  
34  
35  
36  
37  
38  
39  
40  
41  
42  
43  
44  
45  
46  
47  
48  
49  
50  
51  
52  
53  
54  
55  
56  
57  
58  
59  
60

For Peer Review Only

1  
2  
3  
4  
5  
6  
7  
8  
9  
10  
11  
12  
13  
14  
15  
16  
17  
18  
19  
20  
21  
22  
23  
24  
25  
26  
27  
28  
29  
30  
31  
32  
33  
34  
35  
36  
37  
38  
39  
40  
41  
42  
43  
44  
45  
46  
47  
48  
49  
50  
51  
52  
53  
54  
55  
56  
57  
58  
59  
60

## TABLES:

**Table 1**

Parameters in Eqn. 5:	Values used:
$(h, l)$	$(2\text{\AA}, 1\text{\AA})$
$(k_h, k_s)$	$(50 \text{ kcal mol}^{-1} \text{ rad}^{-2}, 10,000 \text{ kcal mol}^{-1} \text{ \AA}^{-2})$ or $(10,000 \text{ kcal mol}^{-1} \text{ rad}^{-2}, 50 \text{ kcal mol}^{-1} \text{ \AA}^{-2})$
$\theta$	$30^\circ, 45^\circ$ or $60^\circ$ (for re-entrant honeycombs) $120^\circ, 135^\circ$ or $150^\circ$ (for non re-entrant honeycombs)

**Table 1: Note that**  $|AA|_0 = |BB|_0 = h$  ,  $|AB|_0 = l$  and  $|A\hat{A}B|_0 = |A\hat{B}B|_0 = \theta$

**Table 2**

Mechanism	Type	$E_y = E_1$ (GPa)	$E_z = E_2$ (GPa)	$\nu_{yz} = \nu_{12}$	$\nu_{zy} = \nu_{21}$	CPU Time (sec)
Hinging	EMUDA (1x1)	752.58	2420.15	-0.536	-1.724	84
	EMUDA (2x2)	752.41	2419.56	-0.536	-1.724	106
	EMUDA (4x4)	752.45	2419.71	-0.536	-1.724	509
	<b>AM</b>	<b>760.00</b>	<b>2540.31</b>	<b>-0.547</b>	<b>-1.828</b>	<i>n/a</i>
Stretching	EMUDA (1x1)	379.10	253.99	0.544	0.365	71
	EMUDA (2x2)	379.04	253.94	0.544	0.365	106
	EMUDA (4x4)	379.04	253.94	0.544	0.365	480
	<b>AM</b>	<b>379.93</b>	<b>254.03</b>	<b>0.547</b>	<b>0.366</b>	<i>n/a</i>

**Table 2: The CPU time and the on-axis Poisson's ratios and Young's moduli for the 'idealised hinging model' and the 'idealised stretching model' with  $\theta = 45^\circ$ , as predicted by the EMUDA model for different sizes of the unit cell relative to the smallest unit cell containing four 'dummy atoms'. Note that despite the differences in the CPU times, the properties of the systems with different unit cell sizes compare very well with each other and the values predicted by the analytical models (AM).**

**Table 3**

$\theta$ (degrees)	Method	$E_y = E_1$ (GPa)	$E_z = E_2$ (GPa)	$\nu_{yz} = \nu_{12}$	$\nu_{zy} = \nu_{21}$
30 <sup>0</sup>	AM	408.00	6301.91	-0.255	-3.928
	EMUDA	407.11	5678.19	-0.251	-3.504
	<i>deviation</i>	-0.22 %	-9.90 %	-1.32 %	-10.81 %
45 <sup>0</sup>	AM	760.00	2540.31	-0.547	-1.828
	EMUDA	752.45	2419.72	-0.536	-1.724
	<i>deviation</i>	-0.99 %	-4.75 %	-1.98 %	-5.72 %
60 <sup>0</sup>	AM	1604.00	1604.27	-1.000	-1.000
	EMUDA	1557.78	1557.80	-0.961	-0.961
	<i>deviation</i>	-2.88 %	-2.90 %	-3.88 %	-3.88 %
120 <sup>0</sup>	AM	963.00	2673.79	0.600	1.667
	EMUDA	934.67	2596.31	0.577	1.602
	<i>deviation</i>	-2.94 %	-2.90 %	-3.88 %	-3.89 %
135 <sup>0</sup>	AM	363.00	5318.99	0.261	3.828
	EMUDA	359.40	5067.11	0.256	3.610
	<i>deviation</i>	-0.99 %	-4.74 %	-1.99 %	-5.71 %
150 <sup>0</sup>	AM	162.00	15927.54	0.101	9.928
	EMUDA	161.11	14353.74	0.099	8.855
	<i>deviation</i>	-0.55 %	-9.88 %	-1.31 %	-10.81 %

**Table 3a: The on-axis Poisson's ratios and Young's moduli for the 'idealised hinging models' as predicted by the analytical model (AM) and as simulated by the EMUDA model, together with the deviations between these values.**

$\theta$ (degrees)	Method	$E_y = E_1$ (GPa)	$E_z = E_2$ (GPa)	$\nu_{yz} = \nu_{12}$	$\nu_{zy} = \nu_{21}$
30 <sup>0</sup>	AM	612.60	286.45	0.764	0.357
	EMUDA	608.13	286.43	0.756	0.356
	<i>deviation</i>	-0.73 %	-0.01 %	-1.00 %	-0.28 %
45 <sup>0</sup>	AM	379.93	254.03	0.547	0.366
	EMUDA	379.04	253.94	0.544	0.365
	<i>deviation</i>	-0.23 %	-0.04 %	-0.50 %	-0.30 %
60 <sup>0</sup>	AM	267.38	267.38	0.333	0.333
	EMUDA	267.20	267.20	0.332	0.332
	<i>deviation</i>	-0.07 %	-0.07 %	-0.34 %	-0.34 %
120 <sup>0</sup>	AM	160.43	445.63	-0.200	-0.556
	EMUDA	160.32	445.34	-0.199	-0.554
	<i>deviation</i>	-0.07 %	-0.07 %	-0.35 %	-0.33 %
135 <sup>0</sup>	AM	181.45	531.9	-0.261	-0.766
	EMUDA	181.03	531.72	-0.260	-0.763
	<i>deviation</i>	-0.23 %	-0.03 %	-0.50 %	-0.30 %
150 <sup>0</sup>	AM	242.38	723.98	-0.302	-0.903
	EMUDA	240.64	723.86	-0.299	-0.900
	<i>deviation</i>	-0.72 %	-0.02 %	-0.98 %	-0.28 %

**Table 3b: The on-axis Poisson's ratios and Young's moduli for the 'idealised stretching models' as predicted by the analytical model (AM) and as simulated by the EMUDA model, together with the deviations between these values.**

**Table 4**

$\theta$ (degrees)	Method	$E_y = E_1$ (GPa)	$E_z = E_2$ (GPa)	$\nu_{yz} = \nu_{12}$	$\nu_{zy} = \nu_{21}$
30 <sup>0</sup>	AM	245.04	274.00	0.15274	0.17079
	EMUDA	245.08	274.04	0.15270	0.17080
	<i>deviation</i>	<i>0.016 %</i>	<i>0.016 %</i>	<i>-0.027 %</i>	<i>0.005 %</i>
45 <sup>0</sup>	AM	253.29	230.94	0.18231	0.16622
	EMUDA	253.35	231.18	0.18200	0.16610
	<i>deviation</i>	<i>0.025 %</i>	<i>0.105 %</i>	<i>-0.168 %</i>	<i>-0.073 %</i>
60 <sup>0</sup>	AM	229.18	229.18	0.14286	0.14286
	EMUDA	229.22	229.22	0.14290	0.14290
	<i>deviation</i>	<i>0.016 %</i>	<i>0.016 %</i>	<i>0.030 %</i>	<i>0.030 %</i>
120 <sup>0</sup>	AM	137.51	381.97	-0.08571	-0.23810
	EMUDA	137.53	382.03	-0.08570	-0.23810
	<i>deviation</i>	<i>0.016 %</i>	<i>0.016 %</i>	<i>-0.017 %</i>	<i>0.002 %</i>
135 <sup>0</sup>	AM	120.97	483.54	-0.08707	-0.34804
	EMUDA	120.64	483.61	-0.08690	-0.34850
	<i>deviation</i>	<i>-0.269 %</i>	<i>0.013 %</i>	<i>-0.193 %</i>	<i>0.133 %</i>
150 <sup>0</sup>	AM	96.95	692.50	-0.06043	-0.43166
	EMUDA	96.97	692.61	-0.06040	-0.43170
	<i>deviation</i>	<i>0.016 %</i>	<i>0.016 %</i>	<i>-0.056 %</i>	<i>0.009 %</i>

**Table 4: The on-axis Poisson's ratios and Young's moduli for the 'hinging + stretching models' as predicted by the analytical model (AM) derived here and as simulated by the EMUDA model, together with the deviations between these values.**

**Table 5**

Parameter SI units (as used in analytical equation)	Parameter in the EMUDA model	Conversion factor	Calculated as ...
$h$ (in m)	$h$ (in Å)	$\times 10^{-10}$	Å $\rightarrow$ m : $\times 10^{-10}$
$l$ (in m)	$l$ (in Å)	$\times 10^{-10}$	Å $\rightarrow$ m : $\times 10^{-10}$
$K_h$ (in J rad <sup>-2</sup> )	$k_h$ (in kcal mol <sup>-1</sup> rad <sup>-2</sup> )	$\times 4184N_A$	kcal $\rightarrow$ J : $\times 4.184 \times 10^3$ 'moles' $\rightarrow$ 'units' : $\times N_A$
$K_s$ (in J m <sup>-2</sup> )	$k_s$ (in kcal mol <sup>-1</sup> Å <sup>-2</sup> )	$\times 4184N_A \times 10^{20}$	kcal $\rightarrow$ J : $\times 4.184 \times 10^3$ 'moles' $\rightarrow$ 'units' : $\times N_A$ Å <sup>-2</sup> $\rightarrow$ m <sup>-2</sup> : $\div (10^{-10})^2$

**Table 5** The conversion factors required for comparing the EMUDA results with those predicted by the analytical model.

FIGURES:

Figure 1

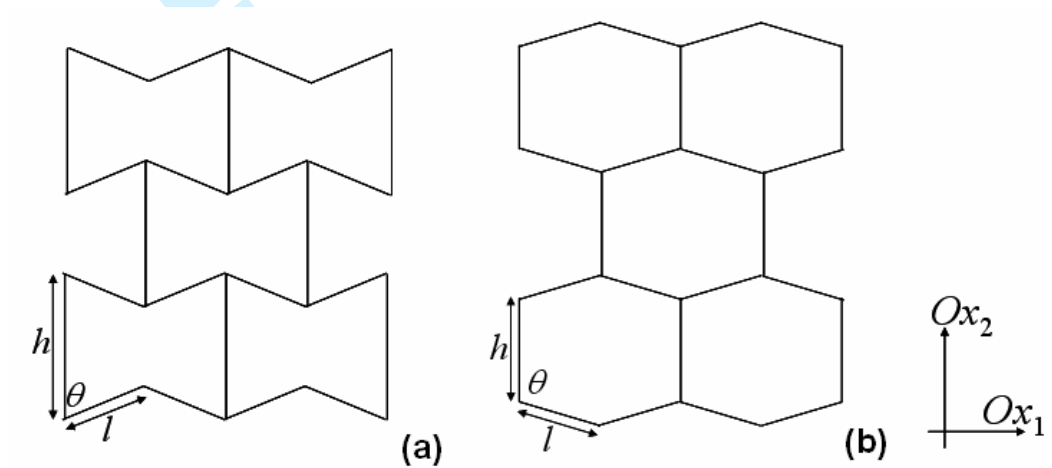


Figure 2

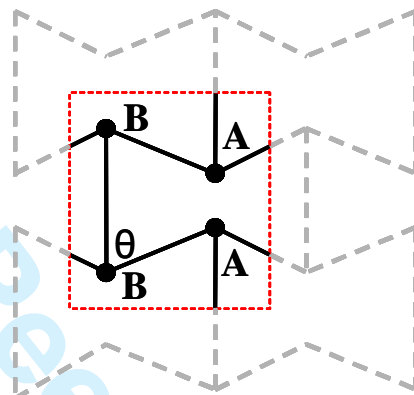
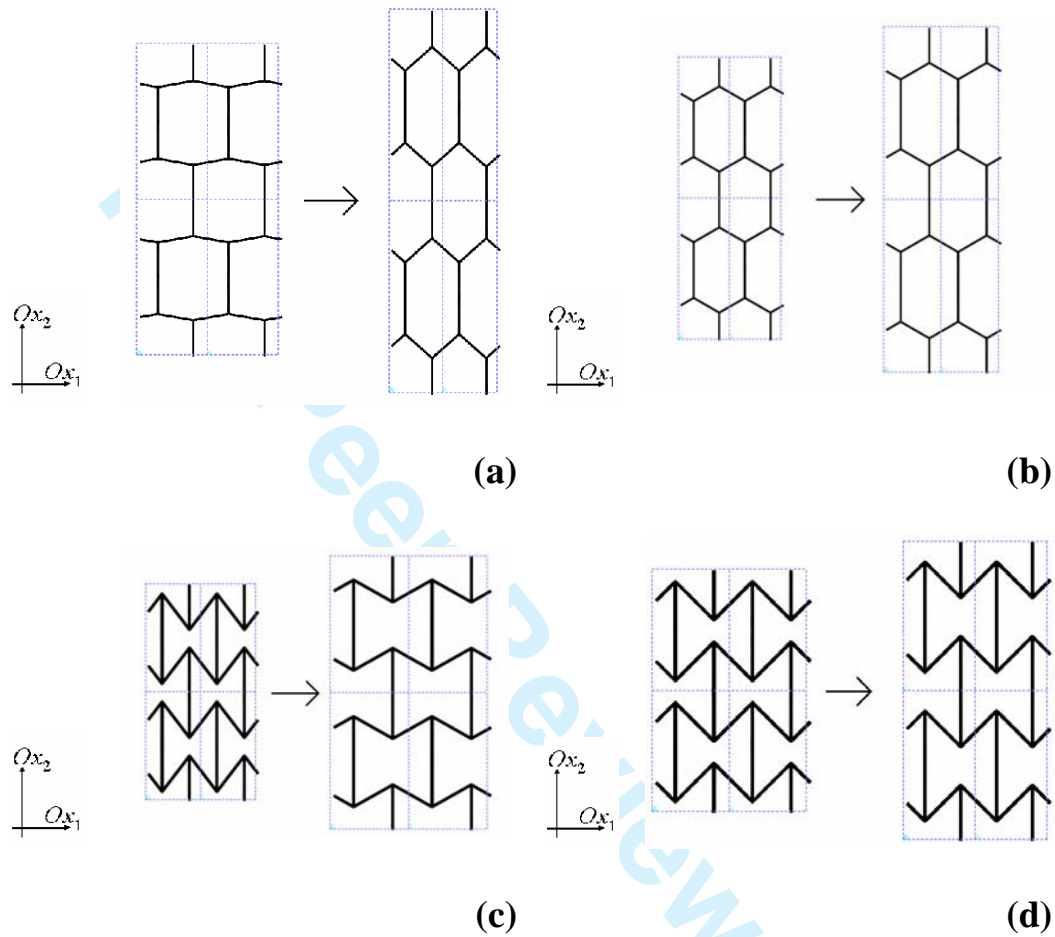


Figure 3





1  
2  
3 Captions:  
4  
5  
6  
7  
8

9 **Figure 1: The (a) re-entrant and (b) non re-entrant hexagonal honeycombs made**  
10 **from rod elements of lengths  $h$  and  $l$  at an angle  $\theta$  to each other. Note that in the**  
11 **EMUDA models, the axes  $Ox_1$  and  $Ox_2$  will be set parallel to the  $Y$  and  $Z$  axes**  
12 **respectively.**  
13  
14  
15  
16  
17

18  
19 **Figure 2: An EMUDA construct of the hexagonal honeycombs built from types**  
20 **of dummy atoms 'A' and 'B'.**  
21  
22  
23  
24  
25

26 **Figure 3: The effect of loads on (a) a non re-entrant honeycomb deforming**  
27 **through hinging; (b) a non re-entrant honeycomb deforming through stretching;**  
28 **(c) a re-entrant honeycomb deforming through hinging, and (d) a re-entrant**  
29 **honeycomb deforming through stretching.**  
30  
31  
32  
33  
34  
35  
36

37 **Figure 4: The percentage differences (absolute values) of the Poisson's ratios**  
38 **from the EMUDA model when compared to the analytical model.**  
39  
40  
41  
42  
43  
44  
45  
46  
47  
48  
49  
50  
51  
52  
53  
54  
55  
56  
57  
58  
59  
60